



Multitarget *in silico* studies of *Ocimum menthiifolium*, family *Lamiaceae* against SARS-CoV-2 supported by molecular dynamics simulation

Amgad Albohy^{a†}, Eman Maher Zahran^{b†}, Usama Ramadan Abdelmohsen^{b,c}, M. Alaraby Salem^d, Tarfah Al-Warhi^e, Mohammad M. Al-Sanea^f, Narek Abelyan^g, Hany Ezzat Khalil^h, Samar Yehia Desoukey^c, Mostafa Ahmed Fouad^c and Mohamed Salah Kamel^{b,c}

^aDepartment of Pharmaceutical Chemistry, Faculty of Pharmacy, The British University in Egypt (BUE), Cairo, Egypt; ^bDepartment of Pharmacognosy, Faculty of Pharmacy, Deraya University, New Minia City, Egypt; ^cDepartment of Pharmacognosy, Faculty of Pharmacy, Minia University, Minia, Egypt; ^dDepartment of Pharmaceutical Chemistry, Faculty of Pharmacy, October University of Modern Sciences and Arts (MSA), Giza, Egypt; ^eDepartment of Chemistry, College of Science, Princess Nourah bint Abdulrahman University, Riyadh, Saudi Arabia; ^fDepartment of Pharmaceutical Chemistry, College of Pharmacy, Jouf University, Aljouf, Saudi Arabia; ^gInstitute of Biomedicine and Pharmacy, Russian-Armenian University, Yerevan, Armenia; ^hDepartment of Pharmaceutical Sciences, College of Clinical Pharmacy, King Faisal University, Hofuf, Saudi Arabia

Communicated by Ramaswamy H. Sarma

ABSTRACT

The novel strain of human coronavirus, emerged in December 2019, which has been designated as SARS-CoV-2, causes a severe acute respiratory syndrome. Since then, it has arisen as a serious threat to the world public health. Since no approved vaccines or drugs has been found to efficiently stop the virulent spread of the virus, progressive inquiries targeting these viruses are urgently needed, especially those from plant sources. Metabolic profiling using LC-HR-ESI-MS of the butanol extract of *Ocimum menthiifolium* (*Lamiaceae*) aerial parts yielded 10 compounds including flavonoids, iridoids and phenolics. As it has been previously reported that some flavonoids can be used as anti-SARS drugs by targeting SARS-CoV-1 3CLpro, we chose to examine 14 flavonoids (detected by metabolomics and other compounds isolated *via* several chromatographic techniques). We investigated their potential binding interactions with the 4 main SARS-CoV-2 targets: M^{Pro}, nsp16/nsp10 complex, ACE2-PD and RBD-S-protein *via* molecular docking. Docking results indicated that the nsp16/nsp10 complex has the best binding affinities where the strongest binding was detected with apigenin-7-*O*-rutinoside, prunin and acaciin with -9.4 , -9.3 and -9.3 kcal/mol binding energy, respectively, compared to the control (SAM) with -8.2 kcal/mol. Furthermore, the stability of these complexes was studied using molecular dynamics of 150 ns, which were then compared to their complexes in the other three targets. MM-PBSA calculations suggested the high stability of acaciin-nsp16 complex with binding energy of -110 kJ/mol. This study sheds light on the structure-based design of natural flavonoids as anti-SARS-CoV-2 drugs targeting the nsp16/10 complex.

Abbreviations: ACE2-PD: Angiotensin converting enzyme 2 protease domain; ARDS: Acute respiratory distress syndrome; COVID-19: Corona virus disease; M^{Pro}: Main protease; MD: Molecular dynamics; PDB: Protein data bank; RBD-S: Receptor binding domain; RMSD: Root mean square deviation; SAM: S-adenosylmethionine; SARS: Severe acute respiratory syndrome

ARTICLE HISTORY

Received 22 June 2020
Accepted 15 November 2020

KEYWORDS

COVID-2; *Ocimum menthiifolium*; flavonoids; molecular docking; molecular dynamics

1. Introduction

Coronaviruses (CoVs), family *Coronaviridae*, are positive-sense-single-stranded, enveloped large RNA viruses ranging in size between 26 kb and 32 kb that infect humans and a wide range of animals and birds (Gurung et al., 2020). The first coronavirus was reported in 1966, and was isolated from patients suffering from common cold. (Bradburne et al., 1967) about 4 decades later, severe outbreak of SARS reported in China in 2002 and spread quickly worldwide, resulting in an 11% mortality rate (Song et al., 2019). In

2012, Middle East respiratory syndrome (MERS) first emerged in Saudi Arabia and subsequently spread to other countries, with a fatality rate of 37% (Hui et al., 2018). Recently, in December 2019, a novel Coronavirus (SARS-CoV-2) causing COVID-19 disease was originated during an outbreak from Wuhan, China (Sang et al., 2020; Xu et al., 2020) and finally, a recent outbreak has emerged in China in January 30, 2020, which became a serious public health emergency of international apprehension (Rodríguez-Morales et al., 2020).

The initial source of SARS-CoV-2 is still unknown, although several studies have suggested that bats may be the

CONTACT Eman Maher Zahran ✉ emanzahran84@yahoo.com 📧 Department of Pharmacognosy, Faculty of Pharmacy, Deraya University, Universities Zone, New Minia City 61111, Egypt

[†]The first and second authors have equal contribution.

📄 Supplemental data for this article can be accessed online at <https://doi.org/10.1080/07391102.2020.1852964>.

© 2020 Deraya University

potential natural host of SARS-CoV-2 (Lu et al., 2020; Zhou et al., 2020). The novel CoV can be transmitted between humans via respiratory droplets with direct or indirect contact with mucous membranes of the eye, mouth or nose, with an incubation period of about 5 days (average 2–14 days) (Lu et al., 2020; Xia et al., 2020). The symptoms start with fatigue, fever, dry cough, myalgia and dyspnea, and advance to have hypoxemia one week after onset, with septic shock, ARDS, metabolic acidosis and coagulation dysfunction, with the danger of high recombination rates arising from high mutation rates of the virus. (Huang et al., 2020; Kumar et al., 2020; Wang et al., 2020). Currently, there are no clinically approved vaccines or specific therapeutic drugs available for COVID-19, together with the serious lacking of clinical investigations (Rodríguez-Morales et al., 2020).

Some preliminary studies have investigated the effectiveness of anti-HIV combination, lopinavir/ritonavir, as a potential inhibitor of SARS-CoV-2 protein synthesis, which is reported to bind to the endopeptidase C30 of SARS-CoV-2 protease as evaluated by molecular models (Lin et al., 2020; Walmsley et al., 2002). Another study suggested the nucleoside analogues, such as Ribavirin, which was broadly used for treatment of SARS patients during the outbreak of SARS in Hong Kong, and Remdesivir which was conveyed to inhibit SARS-CoV and MERS-CoV *in vivo* (Sang et al., 2020). Immunosuppressive drugs as tocilizumab and meplazumab were also surveyed in an open-labeled clinical trial and resulted in a median virus clearance time, discharge time, and a better repair time (Bian et al., 2020; Xu et al., 2020).

Moreover, The antimalarial FDA-approved drug, Chloroquine, has been reported as a potential broad-spectrum antiviral drug *via* effectively suppressing the recently emerged novel CoV (SARS-CoV-2) *in vitro* (Savarino et al., 2006). Undeniably, intensive research on the newly emerged SARS-CoV-2 is urgently needed to elucidate the pathogenic mechanisms and epidemiological characteristics and to face future outbreaks.

Since some bioactive compounds from natural products have been reported to attain antiviral activity, they can be used as a starting point against SARS-CoV-2 (Ul Qamar et al., 2020). Some flavonoids displayed antiviral activity as apigenin, luteolin, quercetin, amentoflavone and kaempferol, which were reported to inhibit the proteolytic activity of SARS-CoV 3CLpro (Jo et al., 2020). Therefore, the antiviral effect is presumed to be directly linked to suppress the activity of SARS-CoV 3CLpro in some cases (Jo et al., 2020). So, we chose 14 bioactive flavonoids, most of them were isolated for the first time *via* metabolic profiling of the *Lamiaceous* plant, *Ocimum menthiifolium*, and proved to have anti-ulcer, local anaesthetic and anti-inflammatory potencies (Zahran et al., 2019; Zahran et al., 2019), and docked them against the 4 main targets: M^{Pro}, nsp16/nsp10 complex, ACE2-PD and RBD-S-protein involved in the Corona infection.

The nsp16 protein is an S-adenosylmethionine (SAM)-dependent methyltransferase which is only activated in the presence of its activating partner nsp10. The activity of nsp16 requires the presence of SAM as a methyl donor which is seen in the active site of the methyl transferase. The methyltransferase catalyzes methylation of the first

transcribed nucleotide at the ribose 2'-O position (2'-O-Me) (Aouadi et al., 2017). The 2'-O-Me of virus cap RNAs shields itself from degradation by 5'-3' exoribonucleases, modify the genetic material of the virus to make it look more like the host (human) cell RNA, and helps to prevent recognition by the host innate immunity (Menachery, Debbink et al., 2014; Menachery, Yount et al., 2014). The inhibition of nsp16/10 2'-O-MTase activities should restrain viral replication and enable recognition by the host innate immune system, making the nsp16/10-MTase a promising target for the identification of new anti-SARS-CoV-2 drugs (Menachery, Yount et al., 2014).

Main protease (M^{Pro}), on the other hand, is a key enzyme which plays a pivotal role in mediating viral replication and transcription, *via* processing the polyproteins that are translated from the viral RNA and disrupting the viral life cycle (Jin et al., 2020). So, inhibition of this enzyme can be a potential target to control SARS-CoV-2 infection as will be discussed. In addition, the integrity of the SARS-CoV particle is maintained *via* four proteins: The S (spike), E (envelop), M (membrane) and N (nucleocapsid) proteins (Han & Král, 2020), where the S protein mediates the entry of the virus into host cells and is recognized by the host angiotensin converting enzyme 2 (ACE2). Based on that, S-protein and ACE2 are considered to play a crucial role in the biology and pathogenesis of SARS-CoV-2 (Li et al., 2003; Wu et al., 2012).

2. Materials and methods

2.1. Plant material

Ocimum menthiifolium aerial parts were collected in September 2016 from the National Garden of Jazan, Jazan KSA. It was identified by Professor Mohamed Abdelhady, Professor of Horticulture, Faculty of Agriculture, Minia University. A voucher specimen (Mn-ph-Cog-038) was reserved in the herbarium of Pharmacognosy Department, Faculty of Pharmacy, Minia University, Egypt.

2.2. Sample preparation and LC-HR-MS coupled metabolic analysis

The butanol extract (3.7 g) of *O. menthiifolium* was subjected to LC-HR-ESI-MS Acquity Ultra Performance Liquid Chromatography system coupled to a Synapt G2 HDMS quadrupole time-of-flight hybrid mass spectrometer (Waters, Milford, USA). A BEH C18 column (2.1 × 100 mm, 1.7 μm particle size; Waters, Milford, USA) is employed for Chromatographic separation, as well as a guard column (2.1 × 5 mm, 1.7 μm particle size) and a linear binary solvent gradient of 0%–100% eluent B over 6 min at a flow rate of 0.3 mL min⁻¹. 0.1% formic acid in water (v/v) was used as solvent A and acetonitrile as solvent B, with injection volume 2 μL and a column temperature of 40 °C. To convert the raw data into separate positive and negative ionization files, Ms converter software was used Using MZmine 2.12 as framework for MS data differential analysis were, the raw data were imported by selecting the ProteoWizard-converted files in mzML format (Ibrahim et al., 2018; Tawfike et al., 2019).

Table 1. Dereplicated compounds from the butanol fr. of *O. menthiifolium*.

No.	Metabolite name	Molecular formula	m/z	Source	Ref.
1	Aucubigenin	C ₉ H ₁₂ O ₄	184.07	<i>Stachys parviflora</i>	(Farooq et al., 2015)
2	Caftaric acid	C ₁₃ H ₁₂ O ₉	312.05	<i>Ocimum basilicum</i>	(Marwat et al., 2011)
3	Gardoside	C ₁₆ H ₂₂ O ₁₀	374.12	<i>Campylanthus glaber</i>	(Rønsted & Jensen, 2002)
4	Salvianolic acid F	C ₁₇ H ₁₄ O ₆	314.08	<i>Melissa officinalis</i>	(Barros et al., 2013)
5	Tuberonic acid glucoside	C ₁₈ H ₂₈ O ₉	388.17	<i>Elsholtzia rugulosa</i>	(Li et al., 2008)
6	Sagerinic acid	C ₃₆ H ₃₂ O ₁₆	720.17	<i>Salvia officinalis</i>	(Lu & Foo, 1999)
7	Prunin	C ₂₁ H ₂₂ O ₁₀	434.12	<i>Ocimum menthiifolium</i>	(Zahran et al., 2020)
8	Acacetin-7-O-glucoside	C ₂₂ H ₂₂ O ₁₀	446.12	<i>Ocimum menthiifolium</i>	(Zahran et al., 2020)
9	Apigenin-7-O-rutinoside	C ₂₇ H ₃₀ O ₁₄	578.16	<i>Ocimum menthiifolium</i>	(Gulluce et al., 2013)
10	Acaciin	C ₂₈ H ₃₂ O ₁₄	576.18	<i>Ocimum menthiifolium</i>	(Gulluce et al., 2013)

Databases as DNP and METLIN were used for dereplicating each *m/z* ion peak (using RT and *m/z* threshold of ± 5 ppm), which provided the putative identities of all metabolomes of the butanol fraction in details (Elsayed et al., 2018).

2.3. Docking studies

The structures of the four target proteins were downloaded from the protein data bank under the following codes: 6LU7, 6W4H, 6VW1 and 6M0J. The structures of the studied ligands were downloaded from PubChem and then subjected to energy minimization using 1000 steps of steepest descent followed by 1000 steps of conjugate gradient algorithms on Avogadro software (Schrodinger, 2010). Water molecules and non-protein residues in each enzyme were removed and hydrogens were added using PyMOL, then the proteins were prepared using Make Macromolecule command on PyRx (Lan et al., 2020; Shang et al., 2020).

For PDB files with multiple conformations, docking was done with both conformations and the best binding energy was reported (Dallakyan & Olson, 2015). The docking calculations were done using AutoDock Vina (Trott & Olson, 2010) using a grid box of 25*25*25 Å³ and exhaustiveness of 16. The grid box was centered on the internal ligand for 6LU7 and 6W4H. For 6VW1, the grid box was centered on residue E35 in the PD region of ACE2. For 6M0J, the grid box was centered on Q493 in the receptor binding domain (RBD) (Forli et al., 2016). When possible, internal ligand was redocked to validate docking method and RMSD value was reported using DockRMSD server (Bell & Zhang, 2019). 3D images were generated using PyMOL (Schrodinger, 2010), while 2D interaction maps were generated using LigPlot Plus (Laskowski & Swindells, 2011).

2.4. MD simulation

Molecular dynamics simulations were performed using GROMACS 2020.2 molecular dynamics package (Abraham et al., 2015). AMBER99SB-ILDN (Lindorff-Larsen et al., 2010) force field was used for simulations. As the forcefield does not contain parameters for the ligand, all ligands were parameterized using ANTECHAMBER to generate parameters that are consistent with the General Amber Force Field (GAFF) (Wang et al., 2004). AM1-BCC method was used to assign charges. ACPYPE was used (Da Silva & Vranken, 2012) for conversion of ligands topologies to format compatible with

GROMACS. All simulations were performed in explicit water environment, using TIP3P model. Complexes were solvated in a dodecahedron box system and were neutralized with the addition of Na⁺ and Cl⁻ ions (Mark & Nilsson, 2001). Steepest descent was used for minimization and Fmax was set of no greater than 1000 kJ mol⁻¹ nm⁻¹. Systems were equilibrated using NVT and NPT ensembles for 200 ps duration each, which was followed by a production run for 150 ns. The temperature in general was sustained at 300 °K using the V-rescale algorithm (Bussi et al., 2007). For the regulation of systems pressure, the Parrinello-Rahman barostat was used (Parrinello & Rahman, 1981). The LINCS (LINear Constraint Solver) algorithm was used for bond's length constraints (Hess et al., 1997). The Particle mesh Ewald (PME) method was used (Darden et al., 1993) for long-range electrostatics calculations. For all simulations timestep was set to 2 fs. Van der Waals cut-off distance was set to 1 nm. Binding free energies were calculated using g_mmpbsa program (Kumari et al., 2014) with MM-PBSA method adapted for GROMACS. In all cases, the predicted binding poses of complexes which are obtained by molecular docking were used as starting points for the corresponding simulations. MD runs were done for compounds 9, 11 and 14 with the 4 protein targets. Co-crystallized ligand if present was used as a control and was run under the same conditions.

2.5. Predicted ADME properties, toxicity profile and target prediction

Investigated compounds were studied for their physicochemical properties and drug likeness using SwissADME server (Daina et al., 2017). Toxicity profiles were predicted by pkCSM Server (Pires et al., 2015) and potential targets were investigated using Swiss Target Prediction (Daina et al., 2017).

3. Results and discussion

3.1. Metabolic profiling

Metabolic profiling of the secondary metabolites of the butanol fraction from *O. menthiifolium* using LC–HR-ESI-MS, resulted in the dereplication of 10 compounds (Table 1) using DNP and METLIN databases. The results revealed the identification of various flavonoids, iridoids and phenolic acids, named as: aucubigenin, caftaric acid, Gardoside, salvianolic acid F, tuberonic acid glucoside, sagerinic acid, prunin, acacetin-7-O-glucoside, apigenin-7-O-rutinoside and acaciin.

The last 4 flavonoids were chosen for docking analysis with 10 other flavonoids previously isolated by us from both the DCM and the ethyl acetate fractions of *O. menthiifolium* via different chromatographic techniques (Zahran et al., 2019, 2020).

3.2. Molecular docking of flavonoids

Isolated bioactive flavonoids (1–14) (Figure 1) were docked against four SARS-CoV-2 potential targets. These targets were previously crystalized and are available through the protein data bank through www.rcsb.org. These targets include the viral main protease (M^{pro} , PDB ID 6LU7), non-structural protein 16/10 complex (nsp16/10) which act as a methyl transferase (PDB ID 6W4H), human angiotensin converting enzyme 2- protease domain (ACE2-PD) which act as a receptor for the virus (PDB ID 6VW1) and the viral recognition binding domain (RBD) of the S protein which recognize its human receptor (PDB ID 6M0J). For the first 2 targets, M^{pro} and nsp16/10 complex, the active site was easily recognized by the presence of a co-crystalized ligand and the docking grid box was centered on the internal ligand. For the other 2 targets, important amino acids that are involved in the interactions between human ACE2-PD and the viral RBD of the S-protein, which include E35 in case of the ACE2 and Q493 in case of the S-protein, were used to center the grid box as reported in previous studies (Shang et al., 2020).

All the isolated compound showed the best binding energies with nsp16/10 complex, moderate affinities with the main protease and much weaker binding with the other two targets (Table 2).

To validate the docking procedure, the co-crystalized ligand (SAM) was redocked in the active site. The docking algorithm was able to reproduce very similar binding mode to the crystal structure with RMSD of 0.233 between the docked and the co-crystalized ligand (Figure 2a). The binding site of the nsp16 is a negatively charged pocket that is formed by specific loops in the protein and shows KDKE methyl transferase motif consisting of Lysine-6844, Aspartic acid-6928, Lysine-6968 and Glutamic acid-7001. The crystal structure shows important interactions of SAM with nsp16 residues (Figure 2b). The purine ring of SAM forms hydrogen bonds with L6898 and C6913 while the methionine part formed four hydrogen bonds with N6841, Y6845, G6879 and D6928. Several other residues involved in the hydrophobic interactions are shown in Figure 2b.

The binding mode of the best docked compounds (**9**, **14** and **11**), takes place in the same position of SAM in a close proximity to the KDKE methyl transferase motif. The carbohydrate part of these 3 compounds extend into a pocket that is formed between two alpha helices, αD and $\alpha 6$ (Figure 3). Apigenin-7-O-rutinoside (**9**) was the highest docked compound with nsp16/10 complex with binding energy of -9.4 Kcal/mol, along with prunin (**11**) and acaciin (**14**), with -9.3 Kcal/mol, for both, compared to the co-crystalized ligand (SAM) which attained -8.2 Kcal/mol, indicating higher binding affinities of the docked compounds. The flavonoid aglycon binds in the same binding site as SAM, where rings

A and B of flavonoid **9** takes the same place of the adenosyl ring of SAM. Ring C of **9** extends into the KDKE methyltransferase motif and forms hydrophobic interactions with K6968 and D6828 of the KDKE motif. The 4'-OH of ring C forms a hydrogen bond with N6841 which is interacting with the methionine carboxylate of SAM in the crystal structure. Rings A and B substituents at 4 and 5 are involved in the hydrogen bond formation with N6899 which is a new interaction that was not seen in the crystal structure, in addition to other hydrogen bonds that are formed with D6912, C6913 and D6931. It worth to mention here that the sugar part especially the terminal moiety extends into a side pocket that is formed between the two alpha helices, αD and $\alpha 6$ and forms a new hydrogen bond interaction with D6931 (Figure 4).

Binding mode of **14** was found to be very similar to that of **9** with most of the hydrogen bonds and hydrophobic interactions conserved (Figure 5a). Binding of **11** is slightly shifted compared to **9** and **14**. The single sugar moiety of **11** takes the same position of the terminal sugar of **9** which causes a shift of the whole flavonoid. Rings A and B are overlapped with the adenine of the SAM while ring C takes the same position of the ribose moiety of SAM (Figure 5b). The compound still shows very similar binding energy (-9.3 kcal/mol) comparable to **9** and **14**.

The results also suggest the importance of the rutinoside moiety in the binding, where two of the best compounds recognized by nsp16, apigenin-7-O-rutinoside (**9**) and Acaciin (**14**), attained the rutinoside moiety. In addition, loss of the terminal rhamnose in **14** decreased the affinity as seen with acacetin-7-O-glucoside (**13**) with a binding energy change of about 0.3 kcal/mol. Further removal of the remaining glucose moiety as seen with the aglycon acacetin (**8**) caused another 1.1 kcal/mol change in the binding energy. This clearly suggest the importance of the sugar moiety of the glycoside in the binding and recognition of nsp16.

Binding of the tested compounds with M^{pro} was generally weaker than that with nsp16/10 but stronger than the other 2 targets. Validation of the docking procedure with M^{pro} was first done via redocking of the internal peptide-like ligand and the correct pose was predicted with good accuracy (RMSD of 1.839 between the docked the crystalized ligand). Among the tested compounds, **9**, **10** and **14** showed the best binding energies with M^{pro} which were higher than that of the internal co-crystalized ligand (Table 2). It worth to mention that every one of these three compounds attains a disaccharide glycone, which suggests the importance of the sugar moiety in the binding of these compounds. The proposed binding mode of all the 3 compounds was found to be very similar. Interactions with the other two targets were much weaker with random binding poses in the grid box which suggest that the compounds do not bind well with these targets.

3.3. Molecular dynamics (MD)

The three compounds with the best docking energies were further investigated and simulated by molecular dynamics with the four SARS-CoV-2 potential protein targets (13

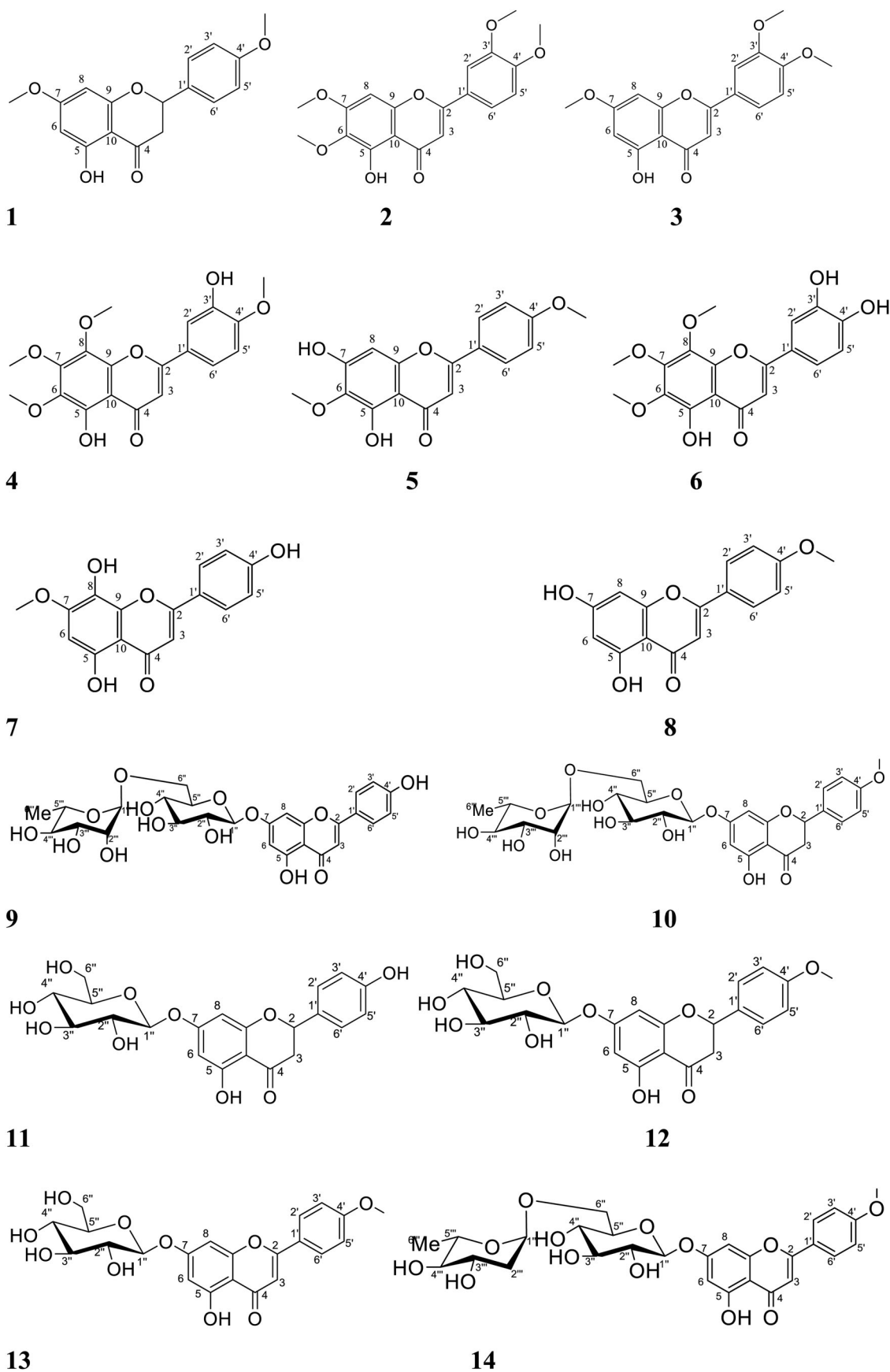


Figure 1. Isolated flavonoids docked against SARS-CoV-2.

Table 2. Docking results of the 14 flavonoids with the 4 main targets of SARS-CoV-2.

	Compounds	M ^{Pro} (6LU7)	NSP16/10 (6W4H)	ACE2-PD (6VW1)	RBD-S- protein (6M0J)
1	Isosakuranetin	-7.3	-7.9	-7.7	-6.1
2	3'-O-methyleupatorin	-7.4	-8.0	-7.2	-6.3
3	5-OH-7,3',4'-trimethoxyflavone	-7.2	-8.2	-6.4	-6.1
4	Gardenin D	-7.3	-7.8	-6.0	-6.2
5	Pectolinarigenin	-7.5	-7.9	-7.1	-6.2
6	Sideritoflavone	-7.2	-7.9	-7.1	-6.2
7	Salvitin	-7.0	-8.0	-7.5	-6.3
8	Acacetin	-7.5	-7.9	-7.6	-6.1
9	Apigenin-7-O-rutinoside	-9.1	-9.4	-6.2	-6.9
10	Didymin	-8.6	-9.2	-6.3	-6.8
11	Prunin	-7.9	-9.3	-6.5	-6.8
12	Isosakuranin	-7.9	-9.0	-6.5	-6.9
13	Acacetin-7-O-glucoside	-8.0	-9.0	-6.6	-7.0
14	Acaciiin	-9.1	-9.3	-6.7	-7.1
	Internal ligand	-7.8	-8.2	-	-

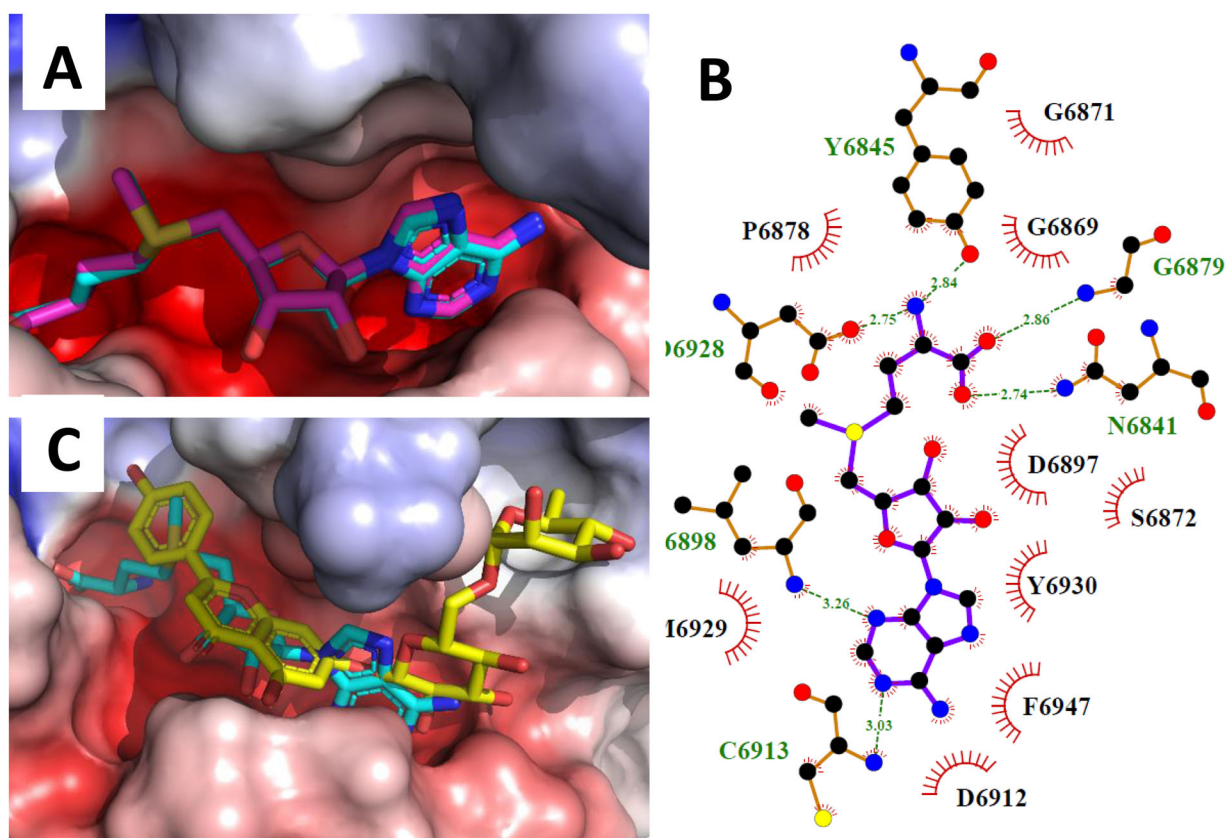


Figure 2. (a) Validation of docking in the active site of nsp16 (6w4H). The figure shows very good overlapping between the crystalized (blue) and docked (pink) S-Adenosyl methionine (SAM). (b) 2D interactions of SAM in the active site of nsp16. (c) Overlapping of **9** with SAM in the active site of nsp16.

protein-ligand complexes, 150 ns each). The RMSDs of all ligands and proteins' alpha carbons were analyzed after fitting the alpha carbons to those of the minimized structures (Figure 6).

Based on the performed molecular dynamics simulations in case of the nsp 16/10 protein, compound **9** showed high stability during simulation, similar to the co-crystallized ligand, SAM, as a control, while the other compounds were relatively less stable compared to both the control and compound **9**. For example, compound **11** is found to leave the active site of nsp16/10 after 130 ns of MD run as seen from the RMSD plot in Figure 6. For RBD-S- protein, compound **11** was relatively more stable during simulation, compared to the other two compounds. In the whole set of simulations of M^{Pro} protein, compound **14** was stable during the whole

length of 150 ns simulation, while compound **11** exhibited stability only at 90 ns. Finally, for ACE2-PD, all the three compounds didn't show that much stability in the active site during the production run.

3.4. Binding free energy calculation

For the detailed analysis of interactions between studied compounds and proteins binding energies were calculated using MM-PBSA method (Table 3). Last 5 ns trajectory of each simulation was used for calculations. Comparative analysis showed that in case of the nsp 16/10 protein, all three studied compounds have better binding energy scores than control compound, SAM (-53 kJ/mol), with compound **14**

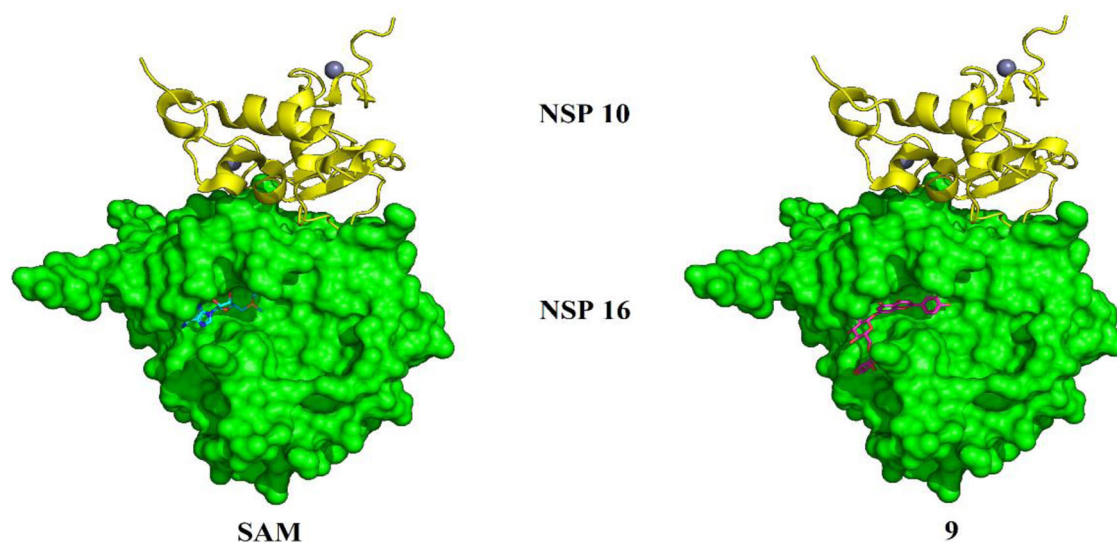


Figure 3. Docking of 9 (pink) takes place in the same groove that is taken by SAM (blue) in the active site of nsp16, compounds 11 and 14 bind at the same pocket. The nsp16/nsp10 complex is exposed where nsp16 is shown as green surface and nsp10 is shown as yellow cartoon.

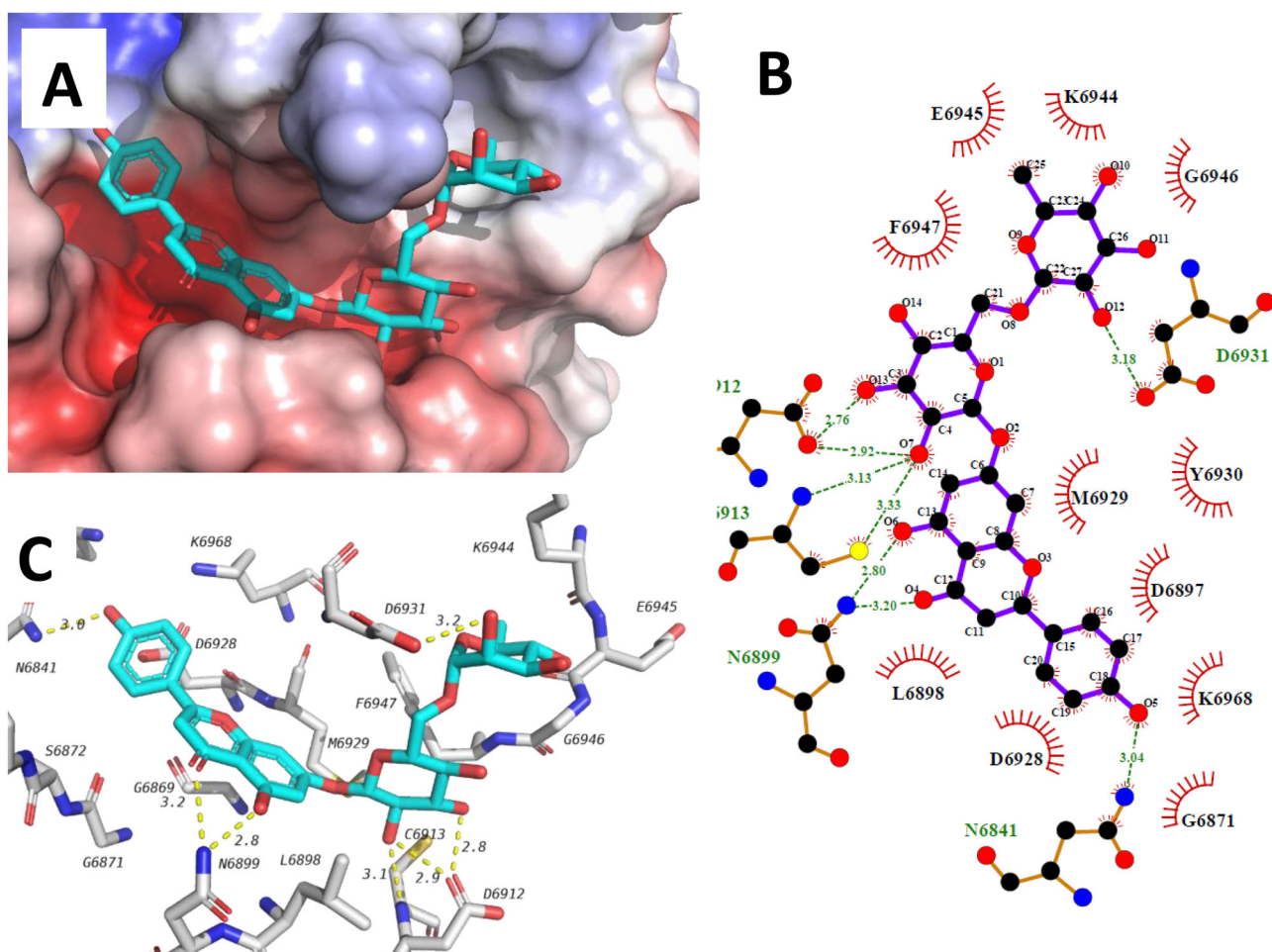


Figure 4. Interactions of Compound 9 in the active site of SARS-CoV-2 nsp16 active site. (a) Compound 9 binding in the same SAM (natural ligand) groove. (b) 2D representation of the amino acids involved in the binding and recognition of compound 9 in the active site. (c) 3D representation of compound 9 interactions.

having lowest binding energy (-110 kJ/mol) and highest affinity. Compound 9 showed highest affinity to 6LU7 and 6M0J proteins, with following binding energies of -85 and -82 kJ/mol, respectively. For 6LU7 protein, compound 14

demonstrated highest binding energy (-115 kJ/mol). Detailed information on interaction types between studied compounds and proteins, and corresponding values are presented in Table 3.

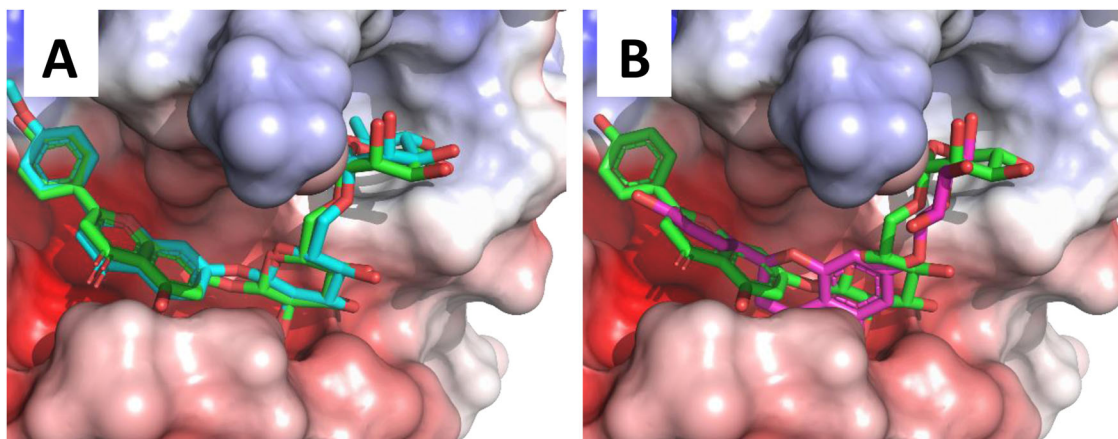


Figure 5. (a) Binding of compound 14 (blue) takes very similar position compared to 9 (green). Both compounds have very similar docking energies. (b) Binding of 11 (pink) is slightly different but maintain key interactions. anti-SARS-CoV-2 drugs targeting the nsp16/10 complex.

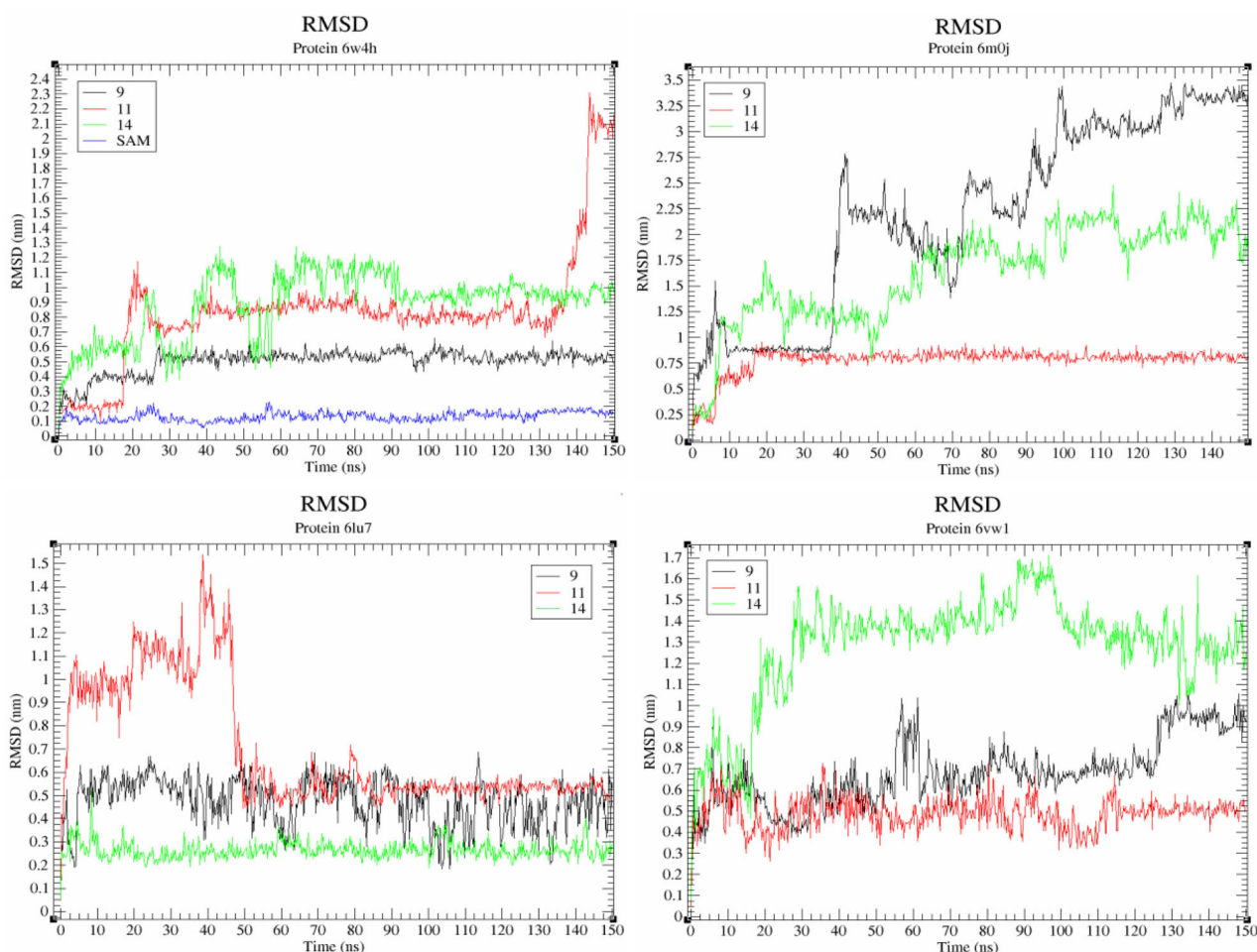


Figure 6. Compounds RMSD values during performed simulations.

3.5. Adme properties, toxicity profiles and target prediction

ADME properties of the investigated compounds were studied to predict the potential route of administration, check if these compounds would be absorbed orally and predict if they would cause any side effects *via* passing the Blood Brain Barrier (BBB). All the investigated compound except compound **3** are not predicted to pass the BBB

which suggest less adverse effects. Non-glycosidic compounds (**1–8**) are orally available while glycosides (**9–14**) are not absorbed orally which might suggest either preparation of prodrugs or changing the route of administration (Supplementary material Table S1). In addition, all compounds are found to obey Lipinski's rule of five except compounds **9**, **10** and **14** which attain a disaccharide moiety.

Table 3. Interactions energies types and values (green to red color gradient represents energy values from maximum to minimum).

Protein	Compound	van der Waal energy (J/mol)	Electrostatic energy (J/mol)	Polar solvation energy (J/mol)	SASA energy (J/mol)	Binding (J/mol)
6W4H	9	-177,530	-73,053	205,721	-18,242	-63,104
	11	-132,690	-33,480	108,306	-12,608	-70,472
	14	-157,300	-139,630	205,302	-19,334	-110,962
6M0J	SAM	-174,460	-289,030	429,307	-18,834	-53,017
	9	-175,510	-88,787	202,258	-20,065	-82,104
	11	-108,530	-43,513	117,018	-12,722	-47,747
6LU7	14	-128,090	-14,161	80,418	-13,179	-75,012
	9	-182,070	-54,962	169,541	-18,400	-85,891
	11	-187,740	-59,367	159,860	-18,370	-105,617
6VW1	14	-242,810	-82,040	231,927	-22,474	-115,397
	9	-116,490	-133,050	195,893	-14,332	-67,979
	11	-99,521	-143,710	216,433	-14,845	-41,643
	14	-82,846	-106,440	159,982	-10,758	-40,062

Toxicity profiles are also predicted through pkCSM Server (Supplementary material Table S2). None of the investigated compounds is predicted to cause skin sensitization or hepatotoxicity. Only compounds **11** and **12** are expected to cause AMES toxicity (test for mutagenic activity) which reflects potential carcinogenicity. Other predicted toxicity tests are shown in Table S2 (Supplementary material).

We also ran a target prediction of top ranked compounds (**9**, **11** and **14**), clearly shown in Tables S3–S5 (Supplementary material). Compounds **9** and **14** are predicted to inhibit TNF- α which might suggest a role in cancer and/or rheumatoid arthritis. None of the tested compounds is predicted to inhibit SARS-CoV-2 targets which is expected since target prediction is based on similarity search (as these targets are newly discovered with no reported inhibitors, so target prediction similarity search will not be able to find such targets). Furthermore, all the three compounds were predicted to interact with Adenosine A1 receptor which is interesting as all of them shares a similar scaffold.

4. Conclusion

A novel severe acute respiratory syndrome coronavirus (SARS-CoV-2) was identified from respiratory illness patients in December 2019 and has recently developed into a serious hazard to the world public health. However, no approved vaccines have been found to efficiently stop the virulent spread of the virus. Given the urgency of the current epidemic situation, it would be highly effective to find bioactive compounds from natural sources and make serious trials and investigations to incorporate them in future plans against COVID. In this study, ten compounds were dereplicated by LC-HR-ESI-MS coupled metabolic profiling of *O. menthaifolium*, ranged between phenolic acids, iridoids and flavonoidal glycosides. Flavonoidal glycosides were chosen along with other flavonoids previously isolated from the same plant and docked against the four main targets involved in SARS-CoV-2. Our results showed that, among all flavonoids tested, apigenin-7-O-rutinoside, prunin and acaciin attained the highest binding affinities towards the nsp16/10 complex. The stability of the docked complexes was further investigated by MD simulations which highlighted Apigenin-7-O-rutinoside to attain the lowest RMSD fluctuation which suggest the high stability of the ligand-protein complex. Acaciin also showed low RMSD fluctuation that took place after 60 ns of the

production run. The MM/PBSA binding energy calculations demonstrated the strong binding of acaciin which showed double the binding energy of the co-crystallized ligand SAM. We also were interested to investigate the drug likeness of the tested compounds as well as their ADMET properties since they could be a potential medication against SARS-CoV-2 (see Supporting Information). This study opens the door for further investigations of these compounds or structurally similar analogues for their use as anti-SARS-CoV-2 medications.

Acknowledgements

The authors extend their appreciation to the Deputyship for Research & Innovation, Ministry of Education in Saudia Arabia for funding this work through the project number 375213500. We also thank Prof. Dr. M. Müller and Prof. Dr. M. Kriskhke for the LC-MS measurement.

Disclosure statement

The authors declare no conflict of interest.

References

- Abraham, M. J., Murtola, T., Schulz, R., Páll, S., Smith, J. C., Hess, B., & Lindahl, E. (2015). GROMACS: High performance molecular simulations through multi-level parallelism from laptops to supercomputers. *SoftwareX*, 1–2, 19–25. <https://doi.org/10.1016/j.softx.2015.06.001>
- Aouadi, W., Blanjoie, A., Vasseur, J.-J., Debart, F., Canard, B., & Decroly, E. (2017). Binding of the methyl donor S-adenosyl-L-methionine to Middle East respiratory syndrome coronavirus 2'-O-methyltransferase nsp16 promotes recruitment of the allosteric activator nsp10. *Journal of Virology*, 91(5), 02217–16. <https://doi.org/10.1128/JVI.02217-16>
- Barros, L., Dueñas, M., Díaz, M. I., Sousa, M. J., Santos-Buelga, C., & Ferreira, I. C. (2013). Phenolic profiles of cultivated, in vitro cultured and commercial samples of *Melissa officinalis* L. infusions. *Food Chemistry*, 136(1), 1–8. <https://doi.org/10.1016/j.foodchem.2012.07.107>
- Bell, E. W., & Zhang, Y. (2019). DockRMSD: An open-source tool for atom mapping and RMSD calculation of symmetric molecules through graph isomorphism. *Journal of Cheminformatics*, 11(1), 40. <https://doi.org/10.1186/s13321-019-0362-7>
- Bian, H., Zheng, Z.-H., Wei, D., Zhang, Z., Kang, W.-Z., Hao, C.-Q., Dong, K., Kang, W., Xia, J.-L., & Miao, J.-L. (2020). Meplazumab treats COVID-19 pneumonia: An open-labelled, concurrent controlled add-on clinical trial. *medRxiv*, 79–91.
- Bradburne, A., Bynoe, M., & Tyrrell, D. (1967). Effects of a "new" human respiratory virus in volunteers. *British Medical Journal*, 3(5568), 767–781. <https://doi.org/10.1136/bmj.3.5568.767>

- Bussi, G., Donadio, D., & Parrinello, M. (2007). Canonical sampling through velocity rescaling. *The Journal of Chemical Physics*, 126(1), 014101. <https://doi.org/10.1063/1.2408420>
- Da Silva, A. W. S., & Vranken, W. F. (2012). ACPYPE - AnteChamber PYthon Parser interface. *BMC Research Notes*, 5(1), 367–377. <https://doi.org/10.1186/1756-0500-5-367>
- Daina, A., Michielin, O., & Zoete, V. (2017). SwissADME: A free web tool to evaluate pharmacokinetics, drug-likeness and medicinal chemistry friendliness of small molecules. *Scientific Reports*, 7, 42717. <https://doi.org/10.1038/srep42717>
- Dallakyan, S., & Olson, A. J. (2015). Small-molecule library screening by docking with PyRx. In *Methods in Molecular Biology* (Vol. 1263). New York, NY: Humana Press. https://doi.org/10.1007/978-1-4939-2269-7_19
- Darden, T., York, D., & Pedersen, L. (1993). Particle mesh Ewald: An N-log(N) method for Ewald sums in large systems. *The Journal of Chemical Physics*, 98(12), 10089–10092. <https://doi.org/10.1063/1.464397>
- Elsayed, Y., Refaat, J., Abdelmohsen, U., Othman, E., Stopper, H., & Fouad, M. (2018). Metabolomic profiling and biological investigation of the marine sponge-derived bacterium *Rhodococcus* sp. UA13. *Phytochemical Analysis*, 29(6), 543–548. <https://doi.org/10.1002/pca.2765>
- Farooq, U., Ayub, K., Hashmi, M. A., Sarwar, R., Khan, A., Ali, M., Ahmad, M., & Khan, A. (2015). A new rosane-type diterpenoid from *Stachys parviflora* and its density functional theory studies. *Natural Product Research*, 29(9), 813–819. <https://doi.org/10.1080/14786419.2014.987775>
- Forli, S., Huey, R., Pique, M. E., Sanner, M. F., Goodsell, D. S., & Olson, A. J. (2016). Computational protein-ligand docking and virtual drug screening with the AutoDock suite. *Nature Protocols*, 11(5), 905–919. <https://doi.org/10.1038/nprot.2016.051>
- Gullecu, M., Orhan, F., Adiguzel, A., Bal, T., Guvenalp, Z., & Dermirezer, L. O. (2013). Determination of antimutagenic properties of apigenin-7-O-rutinoside, a flavonoid isolated from *Mentha longifolia* (L.) Huds. ssp. *longifolia* with yeast DEL assay. *Toxicology and Industrial Health*, 29(6), 534–540. <https://doi.org/10.1177/0748233712442732>
- Gurung, A. B., Ali, M. A., Lee, J., Farah, M. A., & Al-Anazi, K. M. (2020). Unravelling lead antiviral phytochemicals for the inhibition of SARS-CoV-2 Mpro enzyme through in silico approach. *Life Sciences*, 255, 117831. <https://doi.org/10.1016/j.lfs.2020.117831>
- Han, Y., & Král, P. (2020). Computational design of ACE2-based peptide inhibitors of SARS-CoV-2. *ACS Nano*, 14(4), 5143–5147. <https://doi.org/10.1021/acs.nano.0c02857>
- Hess, B., Bekker, H., Berendsen, H. J., & Fraaije, J. G. (1997). LINCS: A linear constraint solver for molecular simulations. *Journal of Computational Chemistry*, 18(12), 1463–1472. [https://doi.org/10.1002/\(SICI\)1096-987X\(199709\)18:12<1463::AID-JCC4>3.0.CO;2-H](https://doi.org/10.1002/(SICI)1096-987X(199709)18:12<1463::AID-JCC4>3.0.CO;2-H)
- Huang, C., Wang, Y., Li, X., Ren, L., Zhao, J., Hu, Y., Zhang, L., Fan, G., Xu, J., Gu, X., Cheng, Z., Yu, T., Xia, J., Wei, Y., Wu, W., Xie, X., Yin, W., Li, H., Liu, M., ... Cao, B. (2020). Clinical features of patients infected with 2019 novel coronavirus in Wuhan. *The Lancet*, 395(10223), 497–506. [https://doi.org/10.1016/S0140-6736\(20\)30183-5](https://doi.org/10.1016/S0140-6736(20)30183-5)
- Hui, D. S., Azhar, E. I., Kim, Y.-J., Memish, Z. A., Oh, M.-d., & Zumla, A. (2018). Middle East respiratory syndrome coronavirus: Risk factors and determinants of primary, household, and nosocomial transmission. *The Lancet. Infectious Diseases*, 18(8), e217–e227. [https://doi.org/10.1016/S1473-3099\(18\)30127-0](https://doi.org/10.1016/S1473-3099(18)30127-0)
- Ibrahim, A. H., Attia, E. Z., Hajjar, D., Anany, M. A., Desoukey, S. Y., Fouad, M. A., Kamel, M. S., Wajant, H., Gulder, T. A. M., & Abdelmohsen, U. R. (2018). New cytotoxic cyclic peptide from the marine sponge-associated *Nocardiosis* sp. UR67. *Marine Drugs*, 16(9), 290–297. <https://doi.org/10.3390/md16090290>
- Jin, Z., Du, X., Xu, Y., Deng, Y., Liu, M., Zhao, Y., Zhang, B., Li, X., Zhang, L., & Peng, C. (2020). Structure of Mpro from COVID-19 virus and discovery of its inhibitors. *bioRxiv*, 3(5), 45–51.
- Jo, S., Kim, S., Shin, D. H., & Kim, M.-S. (2020). Inhibition of SARS-CoV 3CL protease by flavonoids. *Journal of Enzyme Inhibition and Medicinal Chemistry*, 35(1), 145–151. <https://doi.org/10.1080/14756366.2019.1690480>
- Kumar, D., Chandel, V., Raj, S., & Rathi, B. (2020). In silico identification of potent FDA approved drugs against Coronavirus COVID-19 main protease: A drug repurposing approach. *Chemical Biology Letters*, 7(3), 166–175.
- Kumari, R., Kumar, R., Lynn, A., & Open Source Drug Discovery Consortium. (2014). g_mmpbsa-a GROMACS tool for high-throughput MM-PBSA calculations. *Journal of Chemical Information and Modeling*, 54(7), 1951–1962. <https://doi.org/10.1021/ci500020m>
- Lan, J., Ge, J., Yu, J., Shan, S., Zhou, H., Fan, S., Zhang, Q., Shi, X., Wang, Q., Zhang, L., & Wang, X. (2020). Structure of the SARS-CoV-2 spike receptor-binding domain bound to the ACE2 receptor. *Nature*, 581(7807), 215–216. <https://doi.org/10.1038/s41586-020-2180-5>
- Laskowski, R. A., & Swindells, M. B. (2011). LigPlot+: Multiple ligand-protein interaction diagrams for drug discovery. *Journal of Chemical Information and Modeling*, 51(10), 2778–2786. <https://doi.org/10.1021/ci200227u>
- Li, H., Nakashima, T., Tanaka, T., Zhang, Y.-J., Yang, C.-R., & Kouno, I. (2008). Two new maltol glycosides and cyanogenic glycosides from *Elsholtzia rugulosa* Hemsl. *Journal of Natural Medicines*, 62(1), 75–78. <https://doi.org/10.1007/s11418-007-0188-x>
- Li, W., Moore, M. J., Vasilieva, N., Sui, J., Wong, S. K., Berne, M. A., Somasundaran, M., Sullivan, J. L., Luzuriaga, K., Greenough, T. C., Choe, H., & Farzan, M. (2003). Angiotensin-converting enzyme 2 is a functional receptor for the SARS coronavirus. *Nature*, 426(6965), 450–454. <https://doi.org/10.1038/nature02145>
- Lin, S., Shen, R., & Guo, X. (2020). Molecular modeling evaluation of the binding abilities of ritonavir and lopinavir to Wuhan Pneumonia Coronavirus proteases. *bioRxiv*, 1–14.
- Lindorff-Larsen, K., Piana, S., Palmo, K., Maragakis, P., Klepeis, J. L., Dror, R. O., & Shaw, D. E. (2010). Improved side-chain torsion potentials for the Amber ff99SB protein force field. *Proteins*, 78(8), 1950–1958. <https://doi.org/10.1002/prot.22711>
- Lu, C.-w., Liu, X.-f., & Jia, Z.-f. (2020). 2019-nCoV transmission through the ocular surface must not be ignored. *Lancet*, 395(10224), 39–46.
- Lu, R., Zhao, X., Li, J., Niu, P., Yang, B., Wu, H., Wang, W., Song, H., Huang, B., Zhu, N., Bi, Y., Ma, X., Zhan, F., Wang, L., Hu, T., Zhou, H., Hu, Z., Zhou, W., Zhao, L., ... Tan, W. (2020). Genomic characterisation and epidemiology of 2019 novel coronavirus: Implications for virus origins and receptor binding. *The Lancet*, 395(10224), 565–574. [https://doi.org/10.1016/S0140-6736\(20\)30251-8](https://doi.org/10.1016/S0140-6736(20)30251-8)
- Lu, Y., & Foo, L. Y. (1999). Rosmarinic acid derivatives from *Salvia officinalis*. *Phytochemistry*, 51(1), 91–94. [https://doi.org/10.1016/S0031-9422\(98\)00730-4](https://doi.org/10.1016/S0031-9422(98)00730-4)
- Mark, P., & Nilsson, L. (2001). Structure and dynamics of the TIP3P, SPC, and SPC/E water models at 298 K. *The Journal of Physical Chemistry A*, 105(43), 9954–9960. <https://doi.org/10.1021/jp003020w>
- Marwat, S. K., Khan, M. S., Ghulam, S., Anwar, N., Mustafa, G., & Usman, K. (2011). Phytochemical constituents and pharmacological activities of sweet *Basil-Ocimum basilicum* L. (Lamiaceae). *Asian Journal of Chemistry*, 23(9), 3773–3782.
- Menachery, V. D., Debbink, K., & Baric, R. S. (2014). Coronavirus non-structural protein 16: Evasion, attenuation, and possible treatments. *Virus Research*, 194, 191–199. <https://doi.org/10.1016/j.virusres.2014.09.009>
- Menachery, V. D., Yount, B. L., Josset, L., Gralinski, L. E., Scobey, T., Agnihotram, S., Katze, M. G., & Baric, R. S. (2014). Attenuation and restoration of severe acute respiratory syndrome coronavirus mutant lacking 2'-O-methyltransferase activity. *Journal of Virology*, 88(8), 4251–4264. <https://doi.org/10.1128/JVI.03571-13>
- Parrinello, M., & Rahman, A. (1981). Polymorphic transitions in single crystals: A new molecular dynamics method. *Journal of Applied Physics*, 52(12), 7182–7190. <https://doi.org/10.1063/1.328693>
- Pires, D. E., Blundell, T. L., & Ascher, D. B. (2015). pkCSM: Predicting small-molecule pharmacokinetic and toxicity properties using graph-based signatures. *Journal of Medicinal Chemistry*, 58(9), 4066–4072. <https://doi.org/10.1021/acs.jmedchem.5b00104>
- Rodríguez-Morales, A. J., MacGregor, K., Kanagarajah, S., Patel, D., & Schlagenhaupt, P. (2020). Going global—Travel and the 2019 novel coronavirus. *Travel Medicine and Infectious Disease*, 33, 101578. <https://doi.org/10.1016/j.tmaid.2020.101578>

- Rønsted, N., & Jensen, S. R. (2002). Iridoid glucosides and caffeoyl phenylethanoid glycosides from *Campylanthus salsaloides* and *Campylanthus glaber*. *Biochemical Systematics and Ecology*, 30(11), 1091–1095. [https://doi.org/10.1016/S0305-1978\(02\)00061-3](https://doi.org/10.1016/S0305-1978(02)00061-3)
- Sang, P., Tian, S.-H., Meng, Z.-H., & Yang, L.-Q. (2020). Anti-HIV drug repurposing against SARS-CoV-2. *RSC Advances*, 10(27), 15775–15783. <https://doi.org/10.1039/D0RA01899F>
- Savarino, A., Di Trani, L., Donatelli, I., Cauda, R., & Cassone, A. (2006). New insights into the antiviral effects of chloroquine. *The Lancet. Infectious Diseases*, 6(2), 67–69. [https://doi.org/10.1016/S1473-3099\(06\)70361-9](https://doi.org/10.1016/S1473-3099(06)70361-9)
- Schrodinger, L. (2010). The PyMOL molecular graphics system. *Version*, 1(5), 1–13.
- Shang, J., Ye, G., Shi, K., Wan, Y., Luo, C., Aihara, H., Geng, Q., Auerbach, A., & Li, F. (2020). Structural basis of receptor recognition by SARS-CoV-2. *Nature*, 581(7807), 221–224. <https://doi.org/10.1038/s41586-020-2179-y>
- Song, Z., Xu, Y., Bao, L., Zhang, L., Yu, P., Qu, Y., Zhu, H., Zhao, W., Han, Y., & Qin, C. (2019). From SARS to MERS, thrusting coronaviruses into the spotlight. *Viruses*, 11(1), 59–69. <https://doi.org/10.3390/v11010059>
- Tawfiq, A., Attia, E. Z., Desoukey, S. Y., Hajjar, D., Makki, A. A., Schupp, P. J., Edrada-Ebel, R., & Abdelmohsen, U. R. (2019). New bioactive metabolites from the elicited marine sponge-derived bacterium *Actinokineospora spheciospongiae* sp. nov. *AMB Express*, 9(1), 12–18. <https://doi.org/10.1186/s13568-018-0730-0>
- Trott, O., & Olson, A. J. (2010). AutoDock Vina: Improving the speed and accuracy of docking with a new scoring function, efficient optimization, and multithreading. *Journal of Computational Chemistry*, 31(2), 455–461. <https://doi.org/10.1002/jcc.21334>
- Ul Qamar, M. T., Alqahtani, S. M., Alamri, M. A., & Chen, L.-L. (2020). Structural basis of SARS-CoV-2 3CLpro and anti-COVID-19 drug discovery from medicinal plants. *Journal of Pharmaceutical Analysis*, 10(4), 313–319. <https://doi.org/10.1016/j.jpha.2020.03.009>
- Walmsley, S., Bernstein, B., King, M., Arribas, J., Beall, G., Ruane, P., Johnson, M., Johnson, D., Lalonde, R., Japour, A., Brun, S., & Sun, E. (2002). Lopinavir–ritonavir versus nelfinavir for the initial treatment of HIV infection. *New England Journal of Medicine*, 346(26), 2039–2046. <https://doi.org/10.1056/NEJMoa012354>
- Wang, D., Hu, B., Hu, C., Zhu, F., Liu, X., Zhang, J., Wang, B., Xiang, H., Cheng, Z., Xiong, Y., Zhao, Y., Li, Y., Wang, X., & Peng, Z. (2020). Clinical characteristics of 138 hospitalized patients with 2019 novel Coronavirus-infected Pneumonia in Wuhan, China. *JAMA*, 323(11), 1061–1069. <https://doi.org/10.1001/jama.2020.1585>
- Wang, J., Wolf, R. M., Caldwell, J. W., Kollman, P. A., & Case, D. A. (2004). Development and testing of a general amber force field. *Journal of Computational Chemistry*, 25(9), 1157–1174. <https://doi.org/10.1002/jcc.20035>
- Wu, K., Peng, G., Wilken, M., Geraghty, R. J., & Li, F. (2012). Mechanisms of host receptor adaptation by severe acute respiratory syndrome coronavirus. *The Journal of Biological Chemistry*, 287(12), 8904–8911. <https://doi.org/10.1074/jbc.M111.325803>
- Xia, J., Tong, J., Liu, M., Shen, Y., & Guo, D. (2020). Evaluation of coronavirus in tears and conjunctival secretions of patients with SARS-CoV-2 infection. *Journal of Medical Virology*, 92(6), 589–594. <https://doi.org/10.1002/jmv.25725>
- Xu, X., Chen, P., Wang, J., Feng, J., Zhou, H., Li, X., Zhong, W., & Hao, P. (2020). Evolution of the novel coronavirus from the ongoing Wuhan outbreak and modeling of its spike protein for risk of human transmission. *Science China Life Sciences*, 63(3), 457–460. <https://doi.org/10.1007/s11427-020-1637-5>
- Xu, X., Han, M., Li, T., Sun, W., Wang, D., Fu, B., Zhou, Y., Zheng, X., Yang, Y., Li, X., Zhang, X., Pan, A., & Wei, H. (2020). Effective treatment of severe COVID-19 patients with tocilizumab. *Proceedings of the National Academy of Sciences of the United States of America*, 117(20), 10970–10975. <https://doi.org/10.1073/pnas.2005615117>
- Zahrán, E. M., Abdelmohsen, U. R., Hussein, A. S., Salem, M. A., Khalil, H. E., Yehia Desoukey, S., Fouad, M. A., & Kamel, M. S. (2019). Antiulcer potential and molecular docking of flavonoids from *Ocimum forskolei* Benth., family Lamiaceae. *Natural Product Research*, 7, 1–5. <https://doi.org/10.1080/14786419.2019.1645662>
- Zahrán, E. M., Abdelmohsen, U. R., Shalash, M. M., Salem, M. A., Khalil, H. E., Desoukey, S. Y., Fouad, M. A., Krischke, M., Mueller, M., & Kamel, M. S. (2020). Local anaesthetic potential, metabolic profiling, molecular docking and in silico ADME studies of *Ocimum forskolei*, family Lamiaceae. *Natural Product Research*, 8, 1–5.
- Zhou, P., Yang, X.-L., Wang, X.-G., Hu, B., Zhang, L., Zhang, W., Si, H.-R., Zhu, Y., Li, B., Huang, C.-L., Chen, H.-D., Chen, J., Luo, Y., Guo, H., Jiang, R.-D., Liu, M.-Q., Chen, Y., Shen, X.-R., Wang, X., ... Shi, Z.-L. (2020). A pneumonia outbreak associated with a new coronavirus of probable bat origin. *Nature*, 579(7798), 270–273. <https://doi.org/10.1038/s41586-020-2012-7>